Earth and Planetary Science Letters 405 (2014) 39–51

Contents lists available at ScienceDirect

Earth and Planetary Science Letters

www.elsevier.com/locate/epsl

Silurian high-pressure granulites from Central Qiangtang, Tibet: Constraints on early Paleozoic collision along the northeastern margin of Gondwana

Xiu-Zheng Zhang [a,b], Yong-Sheng Dong [b,*], Cai Li [b], Ming-Rong Deng [b], Le Zhang [b], Wang Xu [b]

[a] State Key Laboratory of Isotope Geochemistry, Guangzhou Institute of Geochemistry, Chinese Academy of Sciences, Guangzhou 510640, PR China
[b] College of Earth Science, Jilin University, Changchun, Jilin 130061, PR China

ARTICLE INFO

Article history:
Received 8 March 2014
Received in revised form 5 August 2014
Accepted 6 August 2014
Available online 30 August 2014
Editor: T.M. Harrison

Keywords:
Tibet
Qiangtang
high-pressure mafic granulite
P–T–t path
zircon U–Pb dating
early Paleozoic orogenesis

ABSTRACT

High-pressure (HP) granulites are commonly regarded as indicators of plate convergence and collision following the subduction of oceanic or continental crust. In this study we report the discovery of Silurian HP basic granulites from Central Qiangtang on the Tibetan Plateau. Detailed petrology and geochronology reveal a three-stage metamorphic history based on inclusions, reaction textures, and garnet zoning patterns. Peak metamorphism at 830–860 °C and 1.15–1.45 GPa (M_1) is defined by high-Ca garnet cores, high-Al clinopyroxene, and high-Na plagioclase. Symplectites or coronas of orthopyroxene + plagioclase ± magnetite around garnet porphyroblasts indicate garnet breakdown reactions at ca. 810–830 °C and 0.65–0.85 GPa (M_2). Kelyphites of amphibole + plagioclase around garnet formed during the cooling process at about 590–650 °C and 0.62–0.82 GPa (M_3). These results help define a sequential P–T path containing near-isothermal decompression (ITD) and near-isobaric cooling (IBC) stages. Identification of mineral inclusion assemblages in zircons dated by U–Pb SHRIMP and LA–ICP–MS reveals peak HP metamorphism at ca. 427–422 Ma, subsequent near-isothermal decompression with associated retrograde reactions at ca. 392–389 Ma, and continued cooling at ca. 360 Ma. The P–T–t path of HP basic granulites reflects collision followed by extensional exhumation during early Paleozoic orogenesis. The present results indicate the occurrence of a collisional event along the northern margin of Indo-Australian Gondwana during the Silurian. Renewed Gondwana-directed subduction and subsequent collision probably led to the opening of the Paleo-Tethys Ocean.

1. Introduction

The Qiangtang, Lhasa, North China, South China, and Tarim blocks, along with several other blocks or terranes, form present day East and Southeast Asia. In the early Paleozoic these blocks or terranes were located along the Indo-Australian margin of northeastern Gondwana (Metcalfe, 2006, 2011a, 2011b, 2013). Separation and northward migration of these blocks or terranes from Gondwana occurred in three phases linked with the successive opening and closure of three intervening Tethyan oceans: the Paleo-Tethys (Devonian–Triassic), Meso-Tethys (late early Permian–Late Cretaceous), and Ceno-Tethys (Late Triassic–Late Cretaceous) (Metcalfe, 2013).

A recent study suggests that the central Qiangtang is a key locality, not only to investigate the evolution of the opening and closure of the Paleo-Tethys Ocean (e.g., Li et al., 1995, 2006; Liang et al., 2012; Liu et al., 2011; Zhai et al., 2011a, 2011b, 2013; Zhang et al., 2014), but also to study the tectonic evolution of the north margin of Gondwana in the early Paleozoic. These studies have delineated the Longmu Co-Shuanghu suture zone (LSSZ) as the in situ boundary between the South and North Qiangtang belt (Li et al., 1995; Liang et al., 2012; Liu et al., 2011; Zhai et al., 2011a, 2011b). The LSSZ has been interpreted to represent the main Paleo-Tethys Ocean (Zhai et al., 2011a, 2011b, 2013; Zhu et al., 2013; Metcalfe, 2013) based on the occurrence of Carboniferous ophiolites (Zhai et al., 2013) and Late Devonian and Permian pelagic radiolarian chert (Zhu et al., 2006). Lu–Hf isochron dating of the eclogites and blueschists (244–223 Ma, Pullen et al., 2008) and zircon SHRIMP U–Pb dating of the eclogites (237–230 Ma, Zhai et al., 2011b) indicate a Late Triassic closure of the Paleo-Tethys along the LSSZ. In addition to rocks related to the Paleo-Tethys Ocean,

* Corresponding author at: College of Earth Science, Jilin University, 2199# Jian-She Street, Chaoyang, District, Changchun 130061, PR China. Tel.: +86 13756550816.
E-mail address: yongshengdong2014@163.com (Y.S. Dong).

http://dx.doi.org/10.1016/j.epsl.2014.08.013
0012-821X/

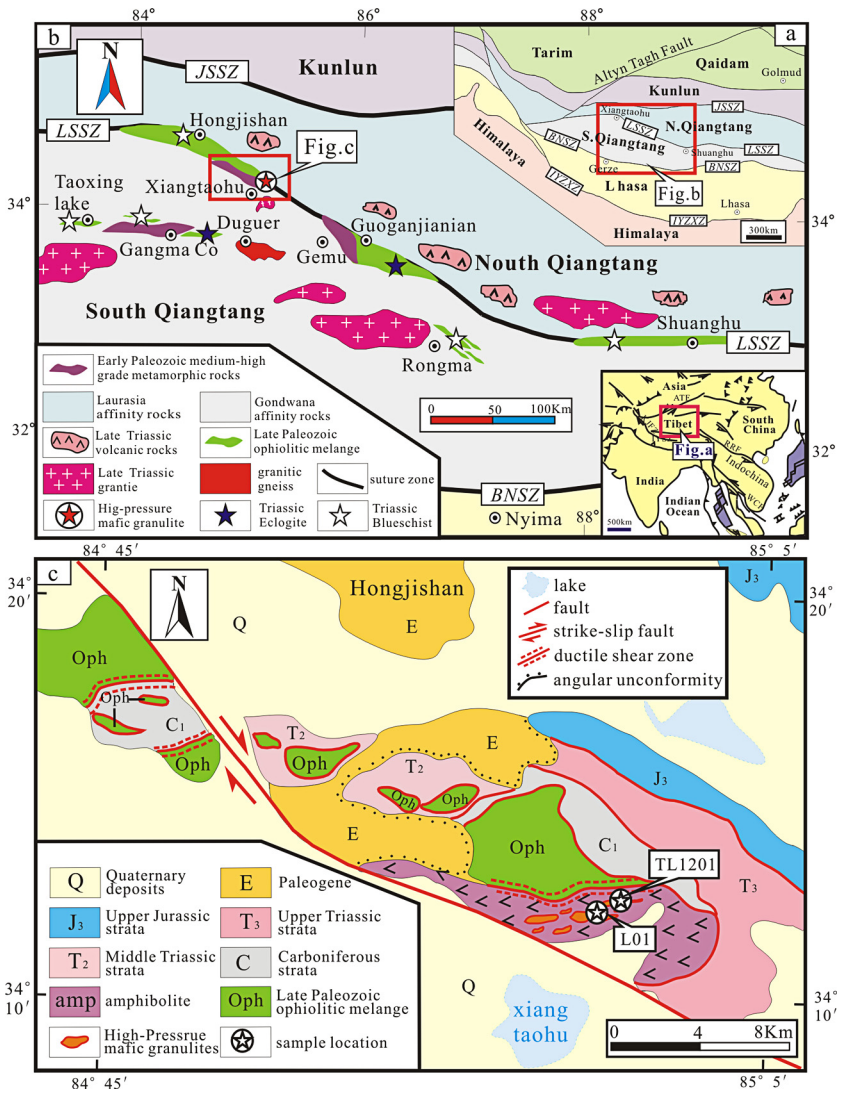

Fig. 1. (a) and (b) Simplified geological map of the Qiangtang area, northern Tibet (modified from Zhai et al., 2011b). (c) Geologic maps of the Xiangtaohu areas, showing outcrops of the HP granulites and the sample locations for zircon dating. JSSZ = Jinsha Suture Zone; LSSZ = Longmu Co-Shuanghu Suture Zone; BNSZ = Bangong-Nujiang Suture Zone; IYZSZ = Indus-Yarlung Zangbo Suture Zone.

geologic evidence of Caledonian tectonism has been reported along the northern margin of South Qiangtang near the LSSZ, including granitic gneiss (ca. 476–471 Ma; Pullen et al., 2011; Hu et al., 2010), amphibolite (± garnet) (ca. 411 Ma, Pullen et al., 2011; ca. 432 Ma, Li et al., 2008), and ophiolites (ca. 517–467 Ma; Wu, 2013; Wang et al., 2013; Zhai et al., 2010). These early Paleozoic rocks indicate the occurrence of earlier tectonothermal events prior to the opening of the Paleo-Tethys Ocean. No reasonable interpretation of the significance of early Paleozoic tectonism has been presented in the literature.

High-pressure granulites, exposed in numerous collisional orogens ranging in age from Archean (e.g. Belomorian tectonic province; Mints et al., 2010) to Cenozoic (e.g. Himalayas; Liu and Zhong, 1997), are important indicators of plate convergence and collision following the subduction of oceanic or continental crust (O'Brien and Rötzler, 2003; Ernst and Liou, 2008). These rocks are frequently interpreted to have formed from the earth's deeper lithosphere and are subject to crustal thickening and thinning processes in continental collisional environments (Brown, 2006; Clarke et al., 2000; Harley, 1989; Möller et al., 2000; O'Brien and Rötzler, 2003). Therefore, pressure–temperature–time (P–T–t) paths of such rocks can be viewed as a record of the thermal and tectonic processes that affected a deeply eroded orogen (Liu et al., 2009).

In this contribution we report on hitherto unknown Silurian HP basic granulites from the Xiangtaohu area of central Qiangtang, northern Tibet. The purpose of this paper is to give a detailed account of the petrological features, mineralogical data, and U–Pb zircon ages for these HP basic granulites. The results are used to constrain the P–T–t paths and metamorphic evolution of the HP rocks, which is critical to understanding the early Paleozoic tectonic history of the Qiangtang terrane. Moreover, the new data allow for the evaluation of hypotheses regarding the evolution of the northeastern margin of Gondwana while providing a starting point for more comprehensive future studies.

2. Geological background and samples

2.1. Regional setting

The Qiangtang terrane is situated in the north–central Tibetan Plateau, bounded by the Jinsha suture to the north and the Bangong-Nujiang suture to the south (Fig. 1a, b) (BGMR, 1993; Tapponnier et al., 1981; Yin and Harrison, 2000). Recent geological studies indicate that the Qiangtang terrane can be subdivided

Fig. 2. Photographs showing field relations between the HP mafic granulites and their country rocks in Xiangtaohu area. (a), (b) HP mafic granulite lenes and blocks in amphibolite; (c), (d) a close-up view of HP mafic granulite and amphibolite.

into the north and south Qiangtang terranes (NQT and SQT) by the Longmu Co-Shuanghu Suture (LSSZ) (Fig. 1a, b) (Li et al., 1995; Liu et al., 2011; Zhai et al., 2011a, 2011b; Zhu et al., 2013), which represents the main Paleo-Tethys Ocean (Zhai et al., 2011a, 2011b, 2013; Zhu et al., 2013; Metcalfe, 2013). The NQT consists of Late Devonian to Triassic sedimentary sequences overlain by Jurassic to Cenozoic sedimentary rocks (BGMR, 1993; Li and Zheng, 1993; Li et al., 1995). Some late Paleozoic sedimentary rocks contain abundant warm-water fossils of Cathaysian affinity (BGMR, 1993; Jin, 2002; Li and Zheng, 1993; Li et al., 1995; Zhang et al., 2009). The SQT consists of both Middle Ordovician–Permian and Jurassic–Cenozoic sedimentary units (BGMR, 1993; Li and Zheng, 1993; Li et al., 1995; Zhang et al., 2009). The Carboniferous to Permian rocks of the SQT are characterized by glaciomarine deposits and cold-water biota, which are typical indicators of a Gondwanan affinity (BGMR, 1993; Jin, 2002; Li and Zheng, 1993; Li et al., 1995; Zhang et al., 2009). Detrital zircon ages from Carboniferous sandstone and quartzite in the SQT are similar to those from Carboniferous strata in the Himalayan and Lhasa terranes (Leier et al., 2007; Pullen et al., 2008).

The LSSZ, proposed by Li (1987) as an in situ Triassic suture zone, extends from northwest to southeast across the Qiangtang Terrane (Fig. 1a, b). It is a tectonic complex composed of blueschist, eclogite, ophiolite, OIB-type basalt, metasedimentary rocks, and minor chert (BGMR, 1993; Li et al., 1995, 2006, 2008; Kapp et al., 2000, 2003; Zhang et al., 2010a, 2010b, 2010c, 2014; Zhai et al., 2007, 2011a, 2011b). The ophiolitic mélange in the LSSZ consists mainly of ultramafic rocks, gabbro, basalt, pillow lava, and minor chert (Zhai et al., 2013). The cumulate gabbros in the Gangma Co and the Guoganjianian areas have recently been dated at ca. 356 Ma and ca. 348–345 Ma, respectively, by U–Pb zircon (SHRIMP) (Zhai et al., 2013). Blueschist and eclogite occurrences have been documented along the LSSZ, including at Gemu, Gangma Co, Rongma, and Shuanghu. The timing of this high-pressure/low-temperature metamorphism has been constrained as Middle to early Late Triassic based on Lu–Hf isochron dating of the eclogites and blueschists (244–223 Ma, Pullen et al., 2008) and U–Pb zircon (SHRIMP) dating of the eclogites (237–230 Ma, Zhai et al., 2011b).

The early Paleozoic relics are mostly exposed along the northern margin of South Qiangtang or within the LSSZ, in the Gangma Co, Xiangtaohu, Duguer, and Guoganjianianshan areas (Pullen et al., 2011; Hu et al., 2010; Li et al., 2008; Zhai et al., 2010). These rocks also experienced a Late Triassic tectonothermal event, and occur as polymetamorphic domains. The available age data include U–Pb zircon ages of 476–464 Ma for granitic gneiss in the Duguer area (Pullen et al., 2011) and 467 Ma for cumulate gabbros in the Taoxing Lake area (Zhai et al., 2010), plus a Lu–Hf mineral isochron age of 411 ± 4 Ma for garnet-bearing amphibolite in the Gangma Co area (Pullen et al., 2008).

2.2. Field occurrence

In this study, we focus on newly discovered Silurian HP basic granulites from the Xiangtaohu area (Fig. 1b, c). The Xiangtaohu granulites are distributed in a 3 km by 200 m belt. These HP basic granulites occur as blocks or lens-shaped bodies of sizes ranging from tens of centimeters to several meters in diameter (Fig. 2a, b, c). The country rock of the HP basic granulite is mainly amphibolite (Fig. 2d). Most blocks or lenses are strongly deformed and exhibit retrograde alteration especially adjacent to the contact with the country rock. Three representative samples of the HP basic granulites (P552b4, P552b5, and L1201b4) were selected for detailed petrological investigation and P–T calculation. Two HP basic granulite samples (TL1201: 34°12′6″ N, 85°00′07″ E; L01: 34°11′52″ N, 84°59′27″ E) were selected for U–Pb zircon dating.

3. Petrography

HP granulite samples investigated in this study are mainly composed of garnet, plagioclase, and clinopyroxene with varying amounts of orthopyroxene, amphibolite, quartz, magnetite, ilmenite, and apatite. In most samples, minor clinopyroxene along

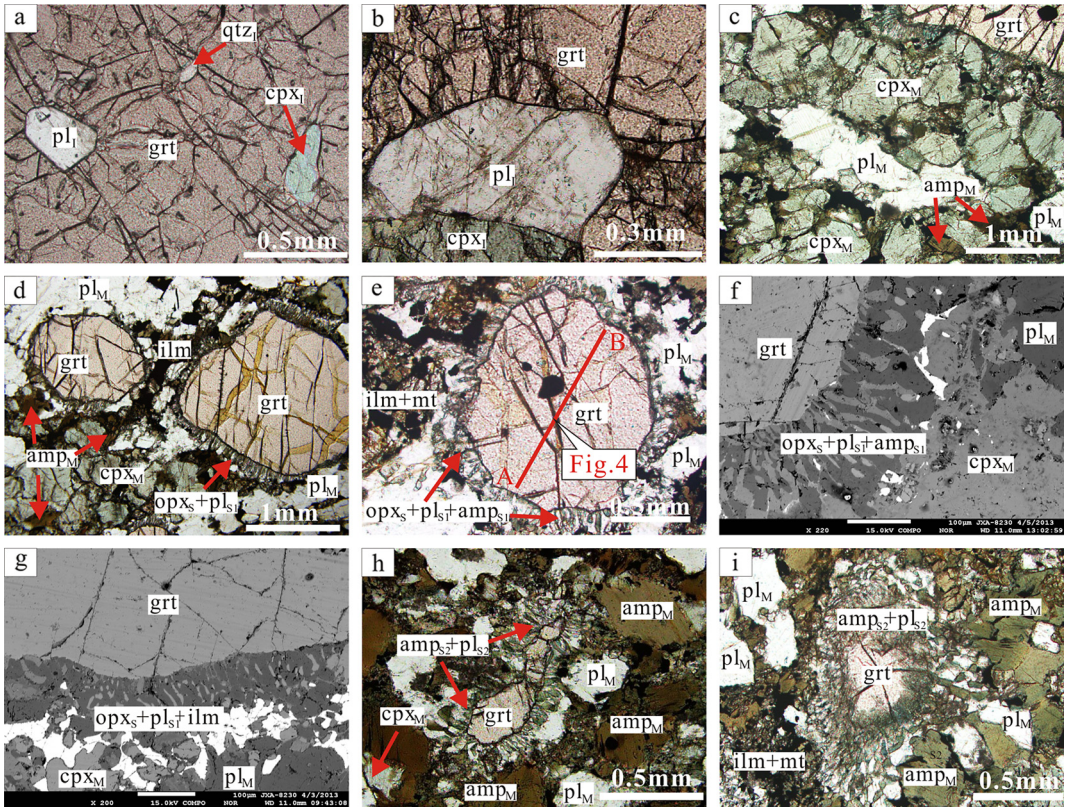

Fig. 3. Photomicrographs and backscattered electron images showing the mineral textures and paragenesis in HP mafic granulites from the Central Qiangtang, Tibetan Plateau. (a), (b) Index HP granulitic mineral assemblage of clinopyroxene + plagioclase ± quartz occurring as inclusions in garnet from sample P552b4 and P552b5 (plane polarized light photomicrograph). (c) The peak mineral assemblage of near-equigranular garnet + clinopyroxene + plagioclase identified in the matrix of sample L1201b4 (plane polarized light photomicrograph). (d), (e) Fine-grained vermicular symplectite of orthopyroxene + plagioclase and orthopyroxene + plagioclase + amphibole around garnet from sample P552b4 (plane polarized light photomicro graph). (f), (g) Symplectite of orthopyroxene + plagioclase + amphibole and orthopyroxene + plagioclase + ilmenite around garnet from sample P552b5 and L1201b4 (BSE image). (h), (i) Symplectite of amphibole + plagioclase around embayed garnet from sample P552b5 and L1201b4 (plane polarized light photomicrograph). Mineral abbreviations: cpx – clinopyroxene, grt – garnet, amp – amphibole, ilm – ilmenite, mt – magnetite, opx – orthopyroxene, pl – plagioclase, qrt – quartz.

with plagioclase, quartz, and apatite occurs as small inclusions in garnet porphyroblasts. Orthopyroxene + plagioclase ± amphibole ± ilmenite symplectites and coronas are present around garnet. Based on inclusions, reaction textures, and compositional profiles of garnet porphyroblasts, three metamorphic stages are recognized: peak (M_1), orthopyroxene + plagioclase-bearing symplectites or coronas (M_2) and amphibole + plagioclase-bearing symplectites and kelyphites (M_3).

3.1. Peak assemblage (M_1)

The peak metamorphic stage is represented by relict inclusion assemblages of Al-rich clinopyroxene (cpx_I), Na-rich plagioclase (pl_I), and quartz (qtz_I) within Ca-rich garnet cores or mantles (Fig. 3a, b), which are essentially unmodified by retrogression. Coarse-grained clinopyroxene and plagioclase in the matrix have been modified significantly from rim to mantle by the effects of decompression and garnet resorption during post-peak (M_2) and retrograde (M_3) metamorphism. Grain interiors, however, are only slightly modified, with compositions similar to those of inclusions. Thus, the relatively Al-rich clinopyroxene cores ($cpx_{M/C}$), Na-rich plagioclase cores ($pl_{M/C}$) and quartz in the matrix, together with Ca-rich garnet cores or mantles, also constitute the peak metamorphic assemblage (Fig. 3c). Apparently, the assemblage garnet + clinopyroxene + plagioclase + quartz dominated the rocks in the peak metamorphic episode. This is a characteristic HP granulite mineral assemblage (Harley, 1989; Carswell and O'Brien, 1993; O'Brien and Rötzler, 2003).

3.2. Orthopyroxene + plagioclase-bearing symplectite or corona (M_2)

The post-peak metamorphic assemblage in most HP granulites investigated here mainly consists of orthopyroxene + plagioclase ± magnetite symplectites and coronas. In most samples, the symplectic texture consists of intergrowths of fine-grained, worm-like orthopyroxene (opx_S) + plagioclase (pl_{S1}) ± magnetite around garnet grains (Fig. 3d, g). Locally, these symplectites completely replace garnet grains and occur as pseudomorphs after garnets. These symplectic or coronitic textures have been observed in many granulite terranes and are generally regarded to indicate that the rock experienced near-isothermal decompression after peak metamorphism (Guo et al., 2002; Harley, 1989, 1992; Thost et al., 1991; Kumar and Chacko, 1994; Carswell and O'Brien, 1993; O'Brien and Rötzler, 2003; Zhao et al., 2001). Rarely, garnet is also surrounded by orthopyroxene (opx_S) + plagioclase (pl_{S1}) + amphibole (amp_{S1}) (Fig. 3e, f). The composition of amp_{S1} differs sharply from that of other later amphiboles (amp_M and amp_{S2}) (Fig. 5f) and this symplectite is usually interpreted to form coevally under the same P–T conditions and controlled by mineral phases adjacent to garnet or the grain-boundary fluid compositions around the garnet (Kumar and Chacko, 1994; Thost et al., 1991; Zhao et al., 2001; Liu et al., 2013). The typical metamorphic reactions between the mineral phases in the M_2 stage are as follows (Harley, 1989; Thost et al., 1991; Liu et al., 2013):

$$grt + cpx + qtz \pm O_2 \rightarrow opx_S + pl_{S1} \pm mt \quad (R_1)$$

$$grt + cpx + qtz + H_2O\,(\text{grain-boundary fluid}) \rightarrow opx_s + pl_{S1} + amp_{S1} + mt \quad (R_2)$$

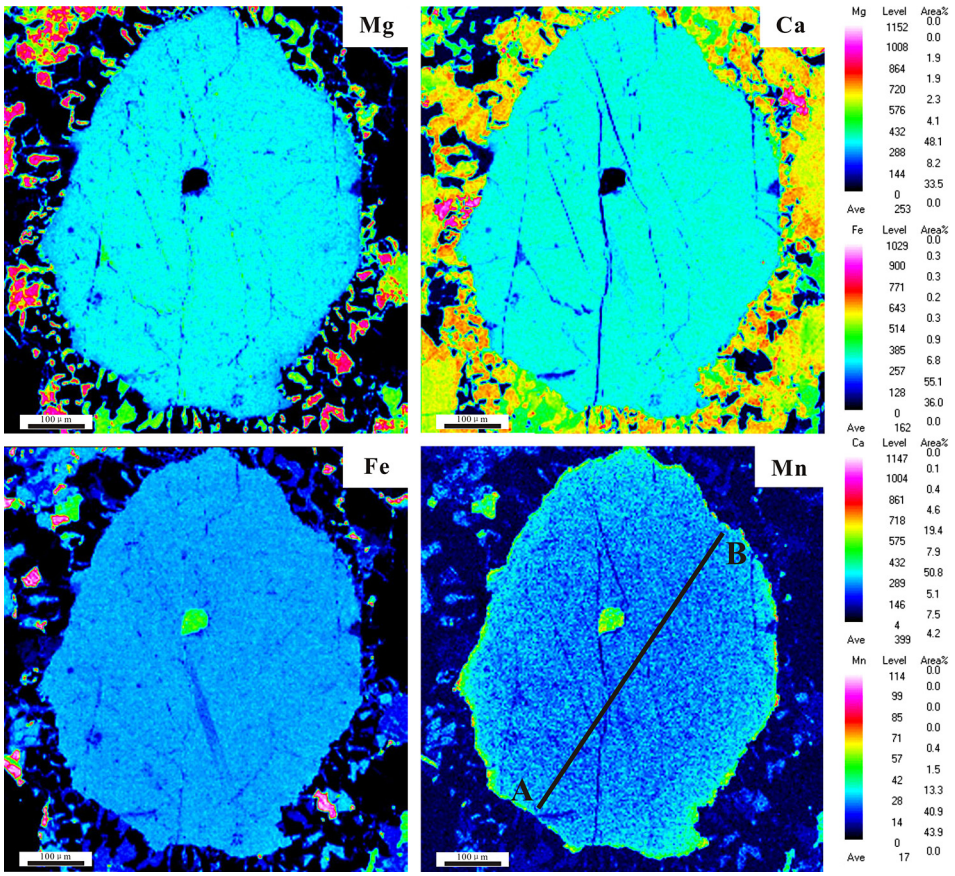

Fig. 4. Compositional maps for the elements Fe, Mg, Ca and Mn in a garnet porphyroblast from samples P552b4 (scale bar = 1.0 mm). A–B is the section line for the compositional profile shown in Fig. 5a.

3.3. *Amphibole + plagioclase-bearing symplectites and kelyphites (M_3)*

The late, amphibolite-facies retrogression stage is represented by kelyphites amphibole (amp_M) and fine-grained symplectites and coronas of amphibole (amp_{S2}) + plagioclase (pl_{S2}) (Fig. 3h, i). In most cases, kelyphites amphibole (amp_M) is developed at the expense of matrix clinopyroxene and surrounds relict M_1 and M_2 pyroxene (Fig. 3h, i) thus confirming their status as the youngest metamorphic indicator mineral. In places, amphibole (amp_{S2}) + plagioclase (pl_{S2}) (Fig. 3h, i) symplectites exhibit a well-developed radial texture or worm-like intergrowth directly adjacent to those embayed garnet grains that lack any orthopyroxene in the corona. The amp_{S2} and amp_M have similar compositions with very low TiO_2 indicating they formed under same metamorphic conditions (Fig. 5f). On the basis of these textures, kelyphites (amp_M) and amphibole (amp_{S2}) + plagioclase (pl_{S2}) symplectites are confirmed as the youngest metamorphic indicator mineral intergrowth and represent an independent metamorphic episode (M_3). The difference in P–T conditions obtained from the two types of symplectite/corona supports this observation. The formation of the amphibolite-facies metamorphic assemblage may be related to the following reactions (Harley, 1989; Liu et al., 2013):

$$cpx + pl + H_2O \rightarrow amp_M \quad (R_3)$$

$$grt + cpx + H_2O \rightarrow amp_{S2} + pl_{S2} \quad (R_4)$$

$$grt + cpx + qtz + H_2O \rightarrow amp_{S2} + pl_{S2} \quad (R_5)$$

4. Mineral chemistry

Three typical samples from the Central Qiangtang were selected for mineral chemical analysis by electron probe micro-analyzer (EPMA) JEOL JXA-8800 at the Institute of Geology and Mineral Resources, Chinese Academy of Geological Sciences (Beijing). The operating conditions were 20 kV, 20 nA beam current, and 5 μm probe diameter. Elemental mapping was performed using a focused beam with 15 kV and 20 nA probe current. X-ray intensities were counted in each 1 μm spot for 0.025 s. Representative mineral analyses are listed in Tables S1–S5. Mineral analyses used for compositional profiles are not shown here. The structural formulae have been given for fixed oxygen values and with Fe^{3+} calculated by stoichiometric charge balance.

4.1. *Garnet*

Representative garnet analyses are given in Table S1. There are: (1) core, mantle and rim compositions of garnet grains surrounded by opx_S + pl_{S1} ± amp_{S1} kelyphites and coronas; (2) core, mantle and rim compositions of garnet grains surrounded by amp_{S2} ± pl_{S2} symplectites. Garnet in the HP granulites consists essentially of almandine (50–54 mol%), grossular (17–21 mol%), and pyrope (24–27 mol%) components with only minor spessartine (1–2 mol%) and andradite (1–3 mol%). Garnet porphyroblasts were compositionally mapped for Mg, Fe, Ca and Mn (Fig. 4), and analyzed by electron microprobe. Nearly all garnet porphyroblasts are compositionally homogeneous or weakly zoned, lacking prograde information (Fig. 4, Fig. 5a). We interpret this zoning pattern to have developed during the peak metamorphism. The outermost rims of garnet in contact with symplectites or coronas have been modified by diffusion and/or a net transfer reaction during post-peak decompression and cooling. There are slight variations in composition among garnets in contact with symplectites or coronas. The compositions of the resetting of garnet-rim (grt_{R1}) in contact with

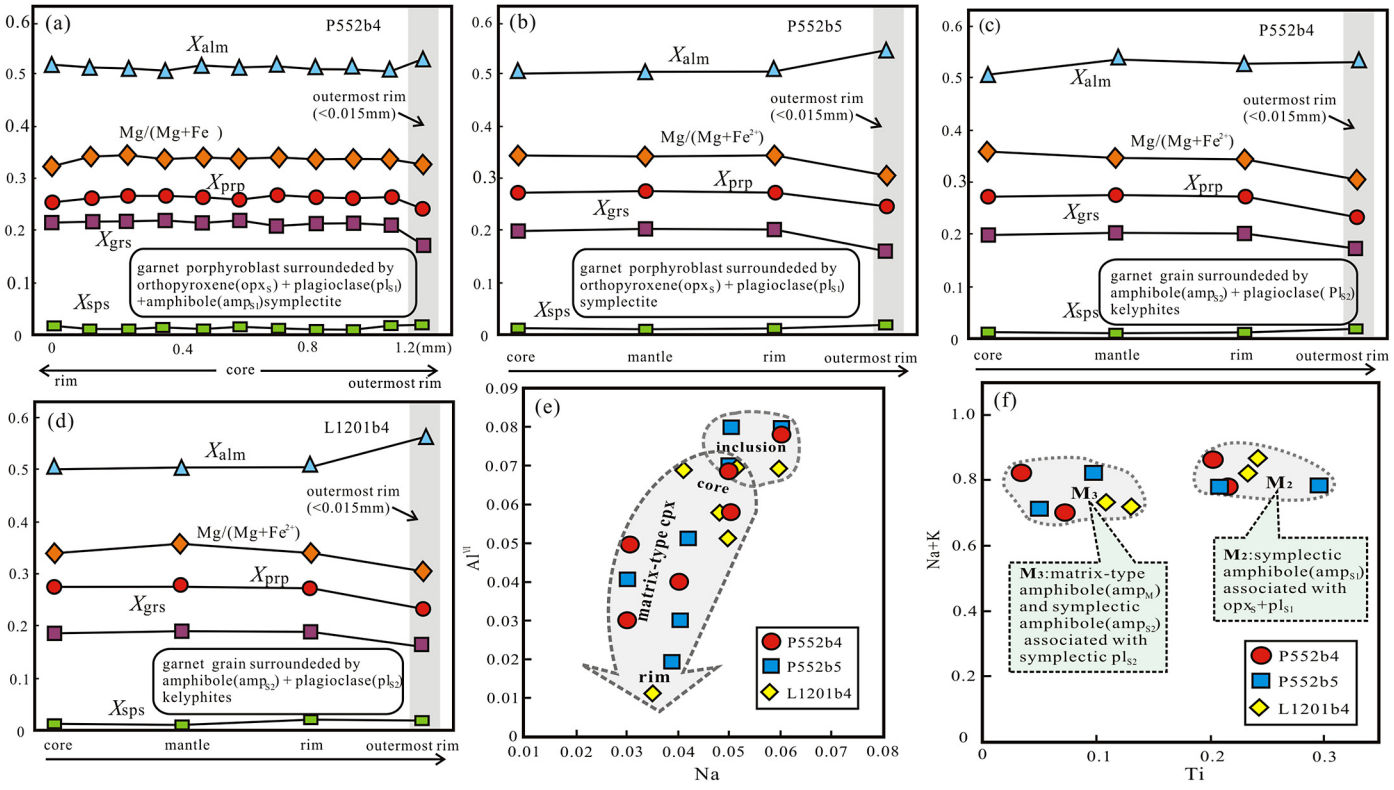

Fig. 5. (a) Core-rim compositional profile for the garnet porphyroblast depicted in Fig. 4; (b), (c) and (d) Core-rim compositional for garnet grains from samples P552b5, P552b4 and L1201b4; (e) Compositions of clinopyroxenes from three different samples plotted in terms of atomic proportions of Na–Al^{VI}, showing variations of these contents from matrix-type grains core to rim, and between clinopyroxene inclusions. (f) Relationship between Ti and (Na + K) of amphibole from different samples, showing variations of amphibole formed at different metamorphic episodes.

$opx_S + pl_{S1} \pm amp_{S1}$ are higher in pyrope and lower in almandine and spessartine than those of the resetting garnet-rim (grt_{R2}) in contact with $amp_{S2} \pm pl_{S2}$ symplectites or coronas (Fig. 5a, b, c, d). These compositional variations imply that the two textural garnets are likely to have re-equilibrated under different conditions.

4.2. Clinopyroxene

Representative clinopyroxene analyses, given in Table S2, include inclusions in garnet and matrix grains. In general, all clinopyroxenes are dominated by a diopside–hedenbergite component together with minor enstatite–ferrosilite and Ca-Tschermaks. One remarkable feature is a large variation in Ca-Tschermaks component which is controlled by Al content. Matrix clinopyroxene shows a sharp core-to-rim decrease in Al_2O_3 from 4.19% to 1.59%. In contrast, clinopyroxene inclusions within garnet porphyroblasts are homogeneous and contain higher Na_2O and slightly higher Al_2O_3 than the cores of matrix clinopyroxene (Fig. 5e). This result suggests that clinopyroxene from the peak metamorphic assemblage (M_1) was more aluminous, as expected for high-pressure/high-temperature conditions (Anovitz, 1991; Carswell and O'Brien, 1993; Cooke, 2000). The considerable drop in Al_2O_3 content from clinopyroxene inclusions in garnet to matrix clinopyroxene (Fig. 5e) is consistent with a significant decrease in pressure and temperature following the metamorphic peak.

4.3. Plagioclase

Table S3 contains representative analyses of: (1) pl_I occurs as inclusions in garnet; (2) matrix-type pl_M; (3) pl_{S1} from $opx_S + pl_{S1} \pm amp_{S1}$ symplectites or coronas; (4) pl_{S2} from $amp_{S2} \pm pl_{S2}$ symplectites. A wide variation in the anorthite content (An_{53-86}) of plagioclase was measured, but there is a distinct textural control on composition. Plagioclase textures include the following: (1) In general, within a single sample, inclusions in garnet have nearly uniform compositions and give the lowest X_{An} values. (2) Plagioclase in the matrix shows a distinct compositional zoning, varying in composition from An_{53} to An_{69}. Higher-An matrix plagioclase occurs along rims in contact with garnet. (3) The X_{An} of symplectic plagioclase is largely dependent on the breakdown of garnet and thus the one directly contacting with the resetting of garnet-rim (grt_{R1} or grt_{R2}) exhibits the highest X_{An}. (4) There is no pronounced compositional difference between plagioclase from $opx_S + pl_{S1} \pm amp_{S1}$ symplectites and that from $amp_{S2} \pm pl_{S2}$ symplectites.

4.4. Amphibole

Amphibole from the high-pressure mafic granulites is calcic-amphibole and three textural kinds of amphiboles are recognized: (1) matrix-type amp_m; (2) symplectic amphiboles (amp_{S1}) from $opx_S + pl_{S1} \pm amp_{S1}$ symplectites or coronas; (3) symplectic amphiboles (amp_{S2}) from $amp_{S2} \pm pl_{S2}$ symplectites. Representative analyses listed in Table S4. According to the nomenclature of Leake et al. (1997), all the amphiboles are pargasite with $T_{Si} = 6.07–6.31$, $(Na + K)_A > 0.5$, $Ti < 0.5$, $Al^{VI} > Fe^{3+}$, and $Mg/(Mg + Fe^{2+}) = 0.55–0.62$. The largest compositional variation in amphibole is that of TiO_2 (Fig. 5f). Most amp_m and amp_{S2} have similar compositions with very low TiO_2 (0.24–1.11 wt.%), but amp_{S1} has a remarkably high TiO_2 content, ranging from 1.73 to 2.65 wt.%. Such differences indicate that amp_{S1} formed at a higher metamorphic grade, probably during post-peak metamorphism (M_2), compared with amp_{S2} and amp_m which formed during retrograde metamorphism (M_3).

4.5. Orthopyroxene

All orthopyroxene in HP granulites from this study occurs in symplectites around garnet. Representative orthopyroxene compositions are listed in Table S5. The symplectic orthopyroxene is high in MgO (18.48–20.42 wt.%) and FeO (25.01–28.08 wt.%), with corresponding Mg/(Mg + Fe) values varying between 0.55 and 0.60. Al_2O_3 is moderate, ranging from 1.21 to 2.81 wt.%.

5. Thermobarometric evaluation

On the basis of petrographic observations of textural relations in the HP granulites from the Xiangtaohu area, three critical mineral paragenesis have been selected in order to determine the P–T conditions for the characteristic metamorphic stages outlined above; namely, garnet + clinopyroxene + plagioclase + quartz, garnet + orthopyroxene + plagioclase + quartz, and garnet + amphibole + plagioclase + quartz.

5.1. Peak HP granulite-facies stage (M_1)

The characteristic peak mineral assemblage is garnet + clinopyroxene + plagioclase ± quartz. In the HP granulites, fine-grained clinopyroxene (with the highest Al and Na contents), plagioclase (with the lowest anorthite content), and quartz occur as inclusions within garnet porphyroblasts and are interpreted to represent the unmodified peak assemblage. Compositions from these inclusions were taken with the garnet cores for P–T calculations of the peak stage of metamorphism (M_1). In addition, the cores of clinopyroxene and plagioclase aggregates adjacent to garnet in the matrix appear to be modified only slightly, giving compositions similar to those of inclusions. These matrix grains were also chosen for calculating the peak P–T conditions of the HP granulite facies stage. P–T conditions were calculated by applying the experimentally and empirically based Fe–Mg exchange thermometers for grt + cpx (Ellis and Green, 1979; Powell, 1985; Krogh, 1988; Ravna, 2000) and geobarometers for the clinopyroxene-bearing assemblage (Newton and Perkins, 1982; Eckert et al., 1991). Seven grt + cpx + pl + qtz determinations from the three HP basic granulite samples (P552b4, P552b5, L1201b1) yielded a P–T range of 1.15–1.45 GPa and 830–860 °C (Table S6), which is representative of the peak conditions of the HP granulite facies stage (M_1) in the Xiangtaohu area.

5.2. Post-peak granulite-facies stage (M_2)

The typical M_2 assemblage contains orthopyroxene and plagioclase, as products of garnet breakdown, developed in symplectites and coronas around garnet porphyroblasts. P–T conditions have been calculated by thermometers for grt + opx (Harley, 1984; Bhattacharya et al., 1991) and geobarometers for the orthopyroxene bearing assemblage (Newton and Perkins, 1982; Bhattacharya et al., 1991), utilizing symplectic orthopyroxene, plagioclase, and the resetting of garnet-rim (grt_{R1}) compositions. Five grt + opx + pl + qtz determinations from the two samples (P552b4, 552b5) yielded a P–T range of 0.65–0.85 GPa and 810–830 °C (Table S6), representing the P–T conditions during the post-peak near-isothermal decompression granulite facies stage (M_2).

5.3. Late amphibolite-facies retrograde stage (M_3)

The representative M_3 assemblage is defined by the appearance of amphibole and plagioclase in hydrous symplectites around garnets. P–T conditions have been calculated using grt + amp thermometry (Graham and Powell, 1984; Ravna, 2000) and geobarometers for the amphibole-bearing assemblage (Kohn and Spear, 1990), utilizing symplectic amphibole, plagioclase, and the resetting of garnet-rim (grt_{R2}) compositions. Four grt + amp + pl + qtz determinations from the two samples (P552b5, L1201b1) yielded a P–T range of 0.62–0.82 GPa and 590–650 °C (Table S6), representing the P–T conditions during the late amphibolite facies retrograde stage (M_3) in the Xiangtaohu HP basic granulites.

6. U–Pb geochronology

6.1. Analytical method

Two samples of HP granulites (TL1201, L01) were selected for in situ zircon U–Pb analysis. For each sample, zircons were separated by conventional heavy liquid and magnetic techniques at the Special Laboratory of the Geological Team of Hebei Province, China. Zircon crystals were embedded in 25 mm epoxy disks and polished down to approximately half the zircon thickness. The zircon CL images were obtained on a FEI PHILIPS XL30 SFEG SEM with 2 min scanning time at conditions of 15 kV and 12 nA at Peking University.

The U–Pb isotope analyses of zircon for sample TL1201 were performed using SHRIMP II at the Beijing SHRIMP Center of Institute of Geology, Chinese Academy of Geological Sciences. Instrumental conditions and measurement procedures were the same as described by Compston et al. (1992). The diameter of the ion beam was 30 μm and the data were collected in sets of five scans through the masses with 2 nA primary O_2 beams. The reference zircon was analyzed first and then after every three unknowns. Standard zircon sample SL13 (572 Ma) was measured to calibrate U, Th and Pb concentrations, and standard zircon TEM (417 Ma) was used for isotopic fractionation correction (Black et al., 2003). The data were processed with the SQUID and ISOPLOT software of Ludwig (1999, 2001). The errors for individual analyses are quoted at the 1σ level, whereas the errors for the weighted mean ages are quoted at 2σ (95% confidence level).

The zircon from sample L01 was analyzed using a current laser ablation plasma mass spectrometric system (LA–ICP–MS) with spot size of 36 μm at the Geological Laboratory Center of China University of Geosciences (Beijing). The analytical method for U–Pb age is the same as those described in Xie et al. (2008). The fractionation correction and results were calculated using GLITTER 4.0 (Jackson et al., 2004) and then corrected using the Harvard zircon 91 500 as external standard. Common Pb was corrected according to the method proposed by Andersen (2002). Uncertainties in age analyses are given as 1σ values, with weighted mean ages quoted at the 95% confidence level. The isotopic data were processed using the GLITTER (version 4.4) and Isoplot/Ex (version 3.0) programs (Ludwig, 2003).

6.2. Mineral inclusions and cathodoluminescence (CL) imaging of zircon

Zircon grains from samples TL1201 and L01 have similar morphologies, showing irregular, rounded, ovoid, and prismatic shapes, lengths that range from 80 to 200 μm, and length-to-width ratios of 1:1 to 1.5:1 (Fig. 6). Based on cathodoluminescence (CL) imaging and crystal habits, these zircon grains can be subdivided into two types. The majority of grains are of type one, characterized by anhedral or subrounded morphology and homogeneous moderate luminescence consistent with a metamorphic origin. Laser Raman spectroscopy reveals the presence of rare mineral inclusions of clinopyroxene, plagioclase, garnet, and quartz. Type two consists of only a few zircon grains from sample TL1201, showing relatively low-luminescence cores, interpreted to be inherited magmatic zircon, surrounded by narrow moderate-to-high-luminescence metamorphic rims.

6.3. Results

6.3.1. SHRIMP dating of sample TL1201

Twenty-seven zircon grains from sample TL1201 were analyzed, and the results are listed in Table S7. In most analyzed gains, U and Th of metamorphic zircon (5–28 ppm and 1–12 ppm, respectively) are lower than those of the magmatic cores (24–124 ppm U and 6–45 ppm Th). The $^{206}Pb/^{238}U$ ages determined for different zircon domains from sample TL1201 can be subdivided into four groups (Table S7; Fig. 7a). Two pre-metamorphic inherited magmatic cores with Th/U ratios of 0.27–0.37 yielded reliable $^{206}Pb/^{238}U$ ages ranging from 481 ± 10 to 500 ± 5 Ma. The majority of uniform metamorphic zircon grains (Th/U = 0.13–0.53) yielded relatively old apparent $^{206}Pb/^{238}U$ ages ranging from 409 ± 12 to 438 ± 13 Ma, with a weighted mean age of 421.5 ± 6.6 Ma ($n = 16$, MSWD = 2.5). The younger metamorphic zircon grains fall into two groups on the basis of $^{206}Pb/^{238}U$ age. The older group (Th/U = 0.35–0.57) yielded $^{206}Pb/^{238}U$ ages ranging from 376 ± 18 to 401 ± 17 Ma with a weighted mean age of 391.6 ± 9.6 Ma ($n = 5$, MSWD = 1.5). The younger group (Th/U = 0.41–0.48) yielded $^{206}Pb/^{238}U$ ages ranging from 359 ± 11 to 370 ± 19 Ma with a weighted mean age of 364.7 ± 7.1 Ma ($n = 4$, MSWD = 0.59).

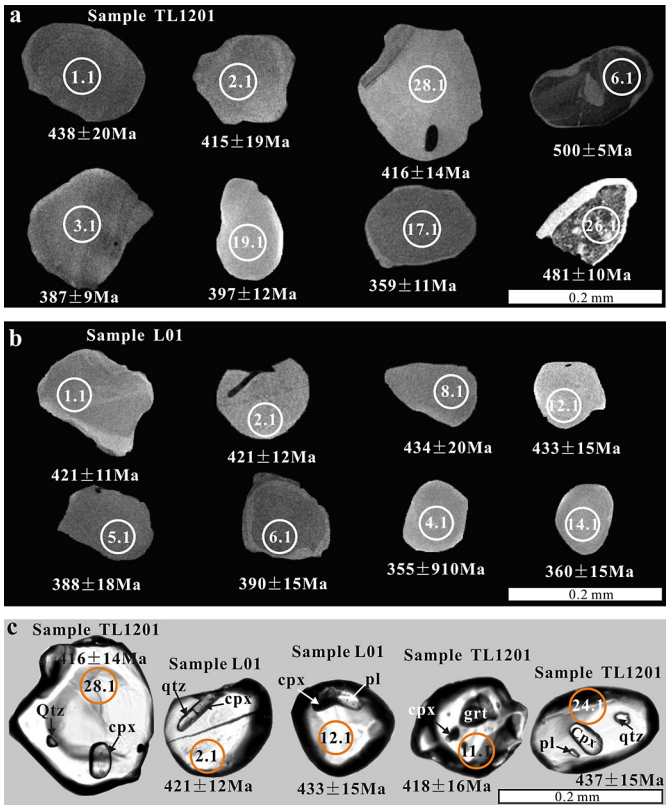

Fig. 6. (a) and (b) CL images showing the internal structure of the analyzed zircon grains from sample TL1201 and L01; (c) Photomicrographs showing typical mineral inclusions (cpx + pl + grt + qtz) in peak metamorphic zircons from the mafic granulite sample TL1201 and L01.

6.3.2. LA–ICP–MS dating of sample L01

Twenty-two zircon grains from sample L01 were analyzed, and the results are listed in Table S8. All the analyses are from homogeneous metamorphic zircon grains, showing variations in U (4–125 ppm) and Th (1–64 ppm) contents, with Th/U ratios ranging from 0.27 to 0.77. $^{206}Pb/^{238}U$ ages can be subdivided into three groups (Fig. 7b). Most zircon yielded relatively old $^{206}Pb/^{238}U$ ages ranging from 421 ± 11 to 435 ± 13 Ma, with a weighted mean age of 427.2 ± 3.9 Ma ($n = 13$, MSWD = 0.62). The second group of zircon grains yielded slightly younger $^{206}Pb/^{238}U$ ages ranging from 388 ± 12 to 399 ± 203 Ma with a weighted mean age of 389.2 ± 4.2 Ma ($n = 7$, MSWD = 0.41). The third group consists of two analyses from sample L01 that yielded $^{206}Pb/^{238}U$ ages of 355 ± 10 and 360 ± 15 Ma.

7. Discussion and conclusions

7.1. Metamorphic evolution of the Qiangtang HP basic granulite

The inherited cores in some zircon domains from the HP basic granulite sample TL1201 are euhedral and prismatic with similar features of magmatic origin (Hoskin and Black, 2000) and yielded $^{206}Pb/^{238}U$ ages from 481 ± 10 to 500 ± 5 Ma. In view of the occurrence of coeval gabbros (517–467 Ma) with similar geochemical features (SSZ-type ophiolite; Wu, 2013; Wang et al., 2013; Zhai et al., 2010) to the Xiangtaohu HP granulites (our unpublished data), we can conclude that these $^{206}Pb/^{238}U$ ages most probably represent the time of the crystallization ages for the protolith of the HP basic granulites. Although most metamorphic zircon from samples TL1201 and L01 have similar characteristics, with irregular or nearly rounded shapes and homogeneous CL zoning, U–Pb analyses define three apparent groups of metamorphic ages: (1) a relatively old weighted mean age of 421.5 ± 6.6 Ma (TL1201) and 427.2 ± 3.9 Ma (L01); (2) a slightly younger weighted mean

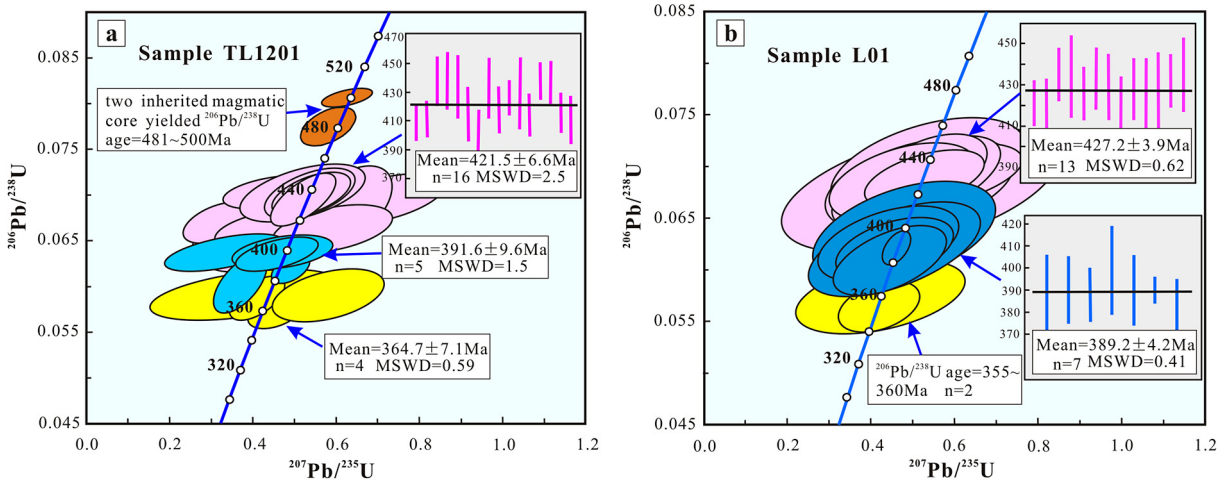

Fig. 7. U–Pb concordia diagrams of zircons for samples TL1201 and L01.

age of 391.6 ± 9.6 Ma (TL1201) and 389.2 ± 4.2 Ma (L01); and (3) the youngest weighted mean age of 364.7 ± 7.1 Ma (TL1201) and $^{206}Pb/^{238}U$ ages ranging from 355 ± 10 to 360 ± 15 Ma (L01). Note that these metamorphic zircons have unusually higher Th/U ratios (Table S7 and Table S8) which are mostly found in zircons of igneous rocks (e.g. gabbros). In fact, these kind of metamorphic zircons with higher Th/U ratios have been observed in many high-grade metamorphic rocks (e.g. granulites and eclogites) (Vavra et al., 1999; Zhai et al., 2011b; Rubatto and Hermann, 2003; Rubatto et al., 1999) and are generally interpreted as the result of the kinetically fast and chemically less selective continuous growth mechanism (Vavra et al., 1999) or the effect of fluid (Rubatto and Hermann, 2003; Rubatto et al., 1999).

Trace element compositions of the zircon (sample L01) analyzed by LA–ICP–MS are summarized in Table S9 and shown in Fig. S1a. The zircon grains with various ages show similar REE patterns are characterized by relatively flat or slightly steep HREE patterns and absence of Eu anomalies (Fig. S1a). Obviously, trace element characteristics of the zircons are not very useful for understanding the origin of these metamorphic zircon grains in our study. The probable cause is that some indicator minerals (e.g. garnet) can exist during different metamorphic episode and the later retrograde stage (M_2 and M_3) did not reach the chemical equilibrium in the whole-rock system.

Mineral inclusions in zircons from high-grade metamorphic rocks are useful for understanding the origin and P–T condition of zircon (re)crystallization (Liu et al., 2004). All the mineral inclusions in zircons from sample TL1201 and L01 were analyzed by Laser Raman spectroscopy, and the results are showed in Fig. S1b and Fig. S1c. It was apparent from the analysis that the oldest group of uniform metamorphic zircon grains from samples TL1201 and L01 contain the inclusion assemblage garnet + clinopyroxene + plagioclase + quartz according with the peak assemblage of HP granulites. The presence of inclusions of the high-pressure granulite facies assemblage suggests that they may grew during peak metamorphism. Therefore, the nearly identical age of ca. 427–422 Ma obtained for these two samples is interpreted to represent the time of the metamorphic peak for the HP basic granulites (M_1). The slightly younger age of ca. 392–389 Ma is confirmed as the age of the later episode of post-peak metamorphism (M_2). It follows that the youngest ages, near 360 Ma, represent an episode of retrograde metamorphism (M_3).

7.2. P–T–t path of HP mafic granulites

The observed petrographic textures, mineral compositions, thermobarometry, and isotopic data of the Xiangtaohu HP basic granulites define a clockwise P–T–t path including near-isothermal decompression, as summarized in Fig. 8. The peak metamorphic stage (M_1), characterized by the mineral assemblage of garnet + clinopyroxene + plagioclase ± quartz, records P–T conditions of 830–860 °C and 1.15–1.45 GPa (Fig. 8). Metamorphic zircons that crystallized in the M_1 stage record the peak high-pressure granulite-facies metamorphic age of ca. 427–422 Ma. The conditions of 810–830 °C and 0.65–0.85 GPa estimated for the orthopyroxene + plagioclase symplectites or coronas assemblage (M_2) suggest near-isothermal decompression from the peak M_1 conditions. Further retrogression and formation of amphibole + plagioclase symplectites (M_3) is estimated to have occurred at 590–650 °C and 0.62–0.82 GPa (Fig. 8). Metamorphic zircons crystallized during the M_2 and M_3 stages record post-peak and further retrogressive ages of ca. 392–389 Ma and ca. 360 Ma.

The HP basic granulites recording relatively high peak P–T conditions and a clockwise P–T path are generally interpreted to indicate subduction/collision-related processes that occurred deep in the lithosphere in the Silurian, followed by subsequent

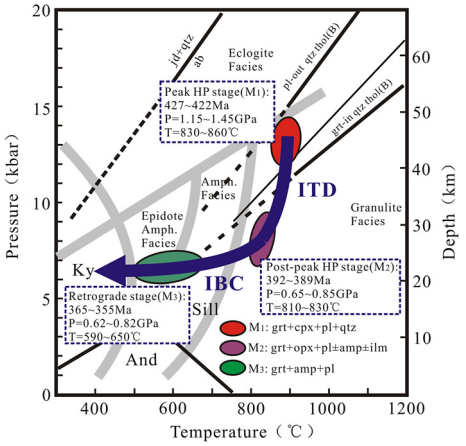

Fig. 8. P–T–t path for HP mafic granulites from the Central Qiangtang, Tibetan Plateau. ab = jd + qtz (Holland, 1980); grt-in and pl-out for quartz tholeiite metabasite composition (Green and Ringwood, 1967); alumino-silicate stability fields (Salje, 1986); fields of metamorphic fades and subfacies (Spear, 1993).

crustal thickening (Brown, 1993, 2001, 2007; England and Thompson, 1984; Harley, 1989, 1992, 2008; O'Brien and Rötzler, 2003; Liu et al., 2009). The high peak P–T conditions implies that protoliths of HP basic granulites experienced burial to depths of ca. 45–50 km and possibly stayed under the peak conditions for a long time forming the homogeneous peak minerals (e.g. garnet). A near-isothermal decompression path and symplectites or coronas widely distributed in HP basic granulites indicates that the rock experienced a rapid exhumation from the depth of 45–50 km to the middle crustal level of 20–25 km. This process likely occurred during collision along a convergent plate margin, followed by extensional exhumation as the collisional orogen collapsed (O'Brien and Rötzler, 2003; Brown, 2006). The M_3 assemblage probably formed when the HP basic granulites were being exhumed to the middle crustal level of ca. 20 km (relatively shallower than those of M_2 stage). Therefore, we suggest that our discovery of HP granulite in Xiangtaohu area may be linked to subduction–collision tectonics, providing robust evidence for the Silurian continental subduction of South Qiangtang.

7.3. Early palaeozoic HP/UHP metamorphism in Gondwana-derived terranes

Although Silurian high-pressure metamorphism in central Qiangtang is first documented in this study, coeval metamorphic events have been reported in the recent literature. Pullen et al. (2008) obtained a Lu–Hf age of ca. 411 Ma for garnet-bearing amphibolite in the Gangma Co area, and Li et al. (2008) reported a U–Pb zircon (SHRIMP) age of ca. 432 Ma for metagabbros from the Guoganjianian area. It is worth noting that the zircon grains from the metagabbros show irregular or nearly rounded shapes and homogeneous CL zoning, similar to HP granulite zircons from this study, consistent with a metamorphic zircon growth. Therefore, the ca. 432 Ma age for the metagabbros in the Guoganjianian area could represent Silurian metamorphism.

Tectono-stratigraphic, paleontological, and paleomagnetic data suggest that the North China, South China, Tarim, South Qiangtang, and several other terranes (Fig. 9) forming present-day East and Southeast Asia were located along the Indo-Australian margin of northeastern Gondwana in the early Paleozoic (Metcalfe, 2006, 2011a, 2011b, 2013). Close faunal affinities suggest contiguity of these continental blocks with each other and with Gondwana from the Cambrian to the Silurian (Rong et al., 1995). Considering the paleogeographic framework of eastern Gondwana, early Paleozoic metamorphic rocks, especially the ultrahigh/high-

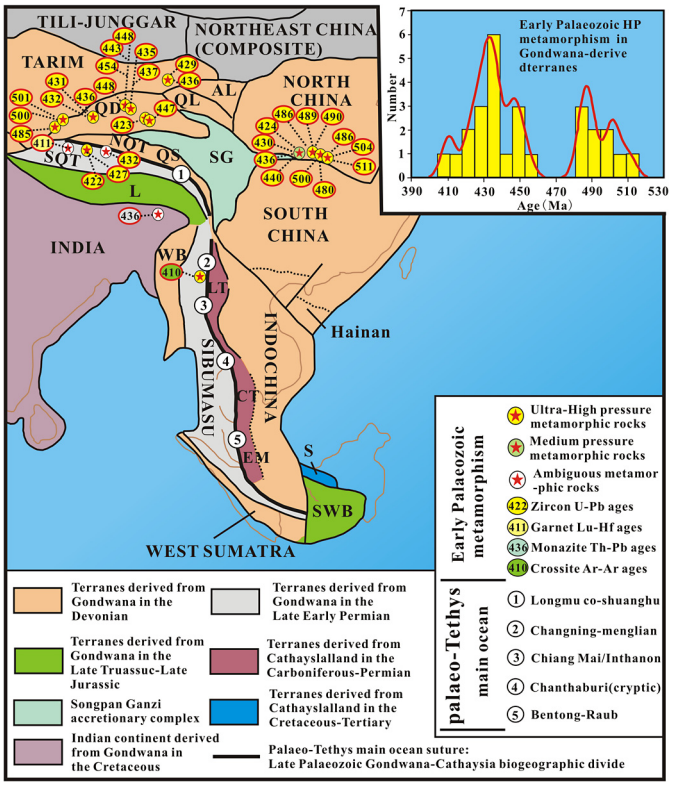

Fig. 9. Distribution of Early Palaeozoic ultrahigh-pressure/pressure metamorphic rocks in principal Gondwana-derived continental blocks or arc terranes (modified from Metcalfe, 2011b). WB = West Burma, SWB = South West Borneo, S = Semitau, L = Lhasa, SQT = South Qiangtang, NQT = North Qiangtang, QS = Qamdo–Simao, SI = Simao, SG = Songpan Ganzi accretionary complex, QD = Qaidam, QI = Qilian, AL = Ala Shan, KT = Kurosegawa Terrane, LT = Lincang arc Terrane, CT = Chanthaburi arc Terrane, EM = East Malaya. Data sources: Tarim (436–429 Ma, Zong et al., 2012), North Qaidam (443–423 Ma; Chen et al., 2007, 2009; Zhang et al., 2008; Song et al., 2006; Yu et al., 2013), the South Altyn (501–485 Ma; Zhang et al., 2005; Liu et al., 2012; Cao et al., 2013), the North Qinling orogen (ca. 511–480 Ma, Liu et al., 2010; Zhang et al., 2011; Wang et al., 2011; Cheng et al., 2011, 2012; ca. 440–424 Ma, Zhang et al., 2011), Sibumasu (ca. 410 Ma, Cong et al., 1993), and Central and Eastern Nepal (ca. 436 Ma, Catlos et al., 2002).

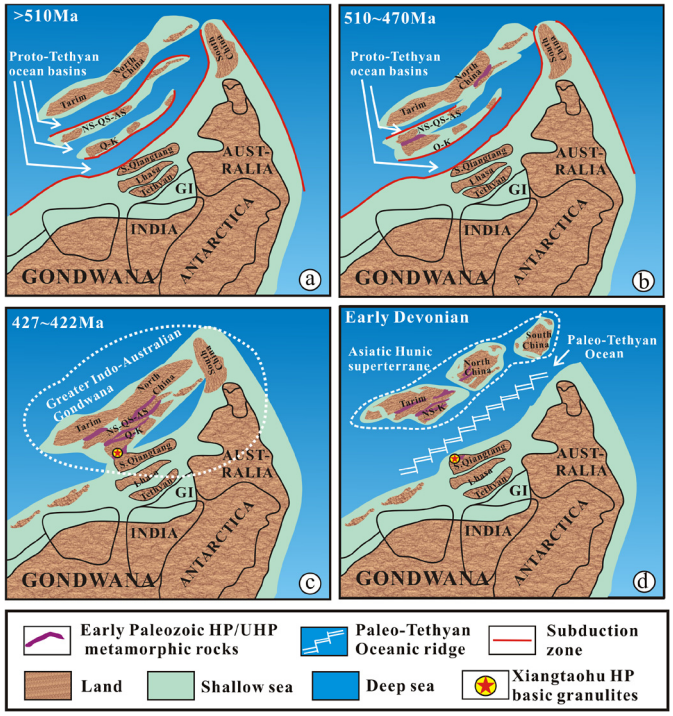

Fig. 10. Schematic illustrations of the nature and evolution of the northern margin of Indo-Australian Gondwana (modified from Gehrels et al., 2011; Metcalfe 2011b, 2013). Q–K = Qaidam–Kunlun terrane, NS–QS–AS = Nan Shan–Qilian Shan–Altun Shan terrane, S. Qiangtang = South Qiangtang, GI = Greater India. Note that these illustrations mainly emphasize the Early Palaeozoic high-pressure/ultrahigh-pressure metamorphic rocks in principal Gondwana-derived terranes, they can be refined and improved with comprehensive comparative studies on early Paleozoic ophiolites and magmatism.

pressure metamorphic rocks, are widespread in most terranes derived from the margin of Indo-Australian Gondwana (Fig. 9), including northeastern Tarim (ca. 436–429 Ma, Zong et al., 2012), North Qaidam (ca. 443–423 Ma; Chen et al., 2007, 2009; Zhang et al., 2008; Song et al., 2006; Yu et al., 2013), the South Altyn (ca. 501–485 Ma; Zhang et al., 2005; Liu et al., 2012; Cao et al., 2013), the North Qinling orogen (ca. 511–480 Ma; Liu et al., 2010; Zhang et al., 2011; Cheng et al., 2011, 2012; Wang et al., 2011; ca. 440–424 Ma, Zhang et al., 2011), Sibumasu (ca. 410 Ma, Cong et al., 1993), and Central and Eastern Nepal (ca. 436 Ma, Catlos et al., 2002).

7.4. Tectonic implications

The Proto-Tethyan margin of Gondwana is commonly considered to have been a passive margin during the early Paleozoic (Debon et al., 1986; Miller et al., 2001). However, this inferred scenario is inconsistent with the evidence of significant early Paleozoic magmatism (530–470 Ma) from most terranes that represent the Proto-Tethyan margin of Gondwana (Cawood et al., 2007; Cawood and Buchan, 2007; Wang et al., 2012; Zhu et al., 2012, 2013). Cawood et al. (2007) argued that on a constant radius earth, the termination of subduction zones within an assembling Gondwana supercontinent (570–510 Ma) must be compensated for by the initiation of subduction zones along the Gondwana Pacific and Proto-Tethyan margins. From this global geodynamic perspective, the early Paleozoic magmatism (ca. 510–470 Ma) in the Himalaya (Cawood et al., 2007; Cawood and Buchan, 2007; Wang et al., 2012), Lhasa (Zhu et al., 2012, 2013; Hu et al., 2013), and South Qiangtang (Pullen et al., 2011; Hu et al., 2010; Zhu et al., 2013) terranes can best be interpreted as a product of the subduction of the Proto-Tethyan oceanic lithosphere beneath the northern margin of Indo-Australian Gondwana. As described by Gehrels et al. (2011), it appears that two other convergent margin systems were present between the northern margin of Indo-Australian Gondwana and outboard micro-continental ribbons (e.g. Tarim–Northern China) during early Paleozoic time:

(1) A north-facing arc, which is interpreted to have brought the Nan Shan–Qilian Shan–Altun Shan terrane juxtaposed with the southern margin of the Tarim craton (Yin and Nie, 1996; Sobel and Arnaud, 1999; Gehrels et al., 2003a, 2003b) (Fig. 10a).

(2) A south-facing system in the Kunlun orogen, which was juxtaposed with the southern margin of the amalgamated Nan Shan–Qilian Shan–Altun Shan–Qaidam–Kunlun terrane (Dewey et al., 1988; Yin and Nie, 1996; Yin and Harrison, 2000) (Fig. 10a).

Numerous, early Paleozoic metamorphic events, in particular the ultrahigh-pressure metamorphism of Gondwana-derived terranes (Fig. 9), indicate the occurrence of a widespread collisional events between the northern margin of Indo-Australian Gondwana and outboard micro-continental ribbons or terrenes during Middle-Late Cambrian to Silurian time.

Our new geochronology results are similar to ages for ultrahigh-pressure metamorphic events in North Qaidam (Chen et al., 2007, 2009; Zhang et al., 2008; Song et al., 2006; Yu et al., 2013) and Tarim (ca. 436–429 Ma, Zong et al., 2012). Citing a presumed Andean-type convergent margin setting along the northern margin of Gondwana (Cawood et al., 2007; Zhu et al., 2013), we propose a hypothetical tectonic model for the early Paleozoic evolution of the

northern margin of Indo-Australian Gondwana. According to our model, the Middle–Late Cambrian to Silurian (ultra)high-pressure metamorphic rocks in these Gondwana-derived terranes formed as a result of successive orogenesis during the accretion of outboard blocks following the subduction of Proto-Tethyan oceanic crust (Fig. 10b, c). These outboard blocks or terranes may have been separated from the northern margin of Gondwana by Proto-Tethyan ocean basins or earlier back-arc basins (Fig. 10a). Collision between these small blocks/terranes and the northern margin of Gondwana may have initiated in the Middle–Late Cambrian (Fig. 9, Fig. 10b) and last to Late Silurian (Fig. 9, Fig. 10c). The main continental fragments collided with the northern margin of Gondwana in the Silurian to form a "Greater Indo-Australian Gondwana" (Fig. 10c). Considering the geochemical characteristics of the Xiangtaohu HP basic granulite (our unpublished data) comparable with those of early Paleozoic ophiolites in central Qiangtang (Wu, 2013; Wang et al., 2013; Zhai et al., 2010), we suggest that the Xiangtaohu HP basic granulites were formed during the closure of the Proto-Tethyan ocean basin or earlier back-arc basin. Renewed subduction of Proto-Tethys crust and subsequent Silurian collision triggered slab break-off, leading to the rapidly erosional exhumation of Xiangtaohu HP basic granulites (ca. 392–389 Ma) and opening of the Paleo-Tethys ocean basin (Fig. 10d). Robust paleomagnetic, biogeographical, and tectonostratigraphic data indicate that the Paleo-Tethyan Ocean initially opened as a back-arc basin during the Middle Silurian to Early Devonian in response to the detachment of the ribbon-like "Asiatic Hunic superterrane" from the northern margin of Gondwana (Fig. 10d) (Stampfli and Borel, 2002; Von Raumer et al., 2002; Ferrari et al., 2008; Lehmann et al., 2013; Metcalfe, 2011b, 2013). The "Asiatic Hunic superterrane" might have been an assemblage of continental blocks or volcanic islands including Tarim–Qaidam, North and South China (Stampfli and Borel, 2002; Von Raumer et al., 2002; Metcalfe, 2011b, 2013). The opening of the Paleo-Tethyan Ocean also led to the arrest and dismemberment of the early Paleozoic orogenesis along the northern margin of Indo-Australian Gondwana. Therefore, relics of the orogen, such as early Paleozoic magmatic arc rocks, ultrahigh-pressure metamorphic rocks, and/or ophiolites, could be preserved in both the separated "Asiatic Hunic superterrane" and the newly formed northern margin of Gondwana (e.g. South Qiangtang).

Although important information from key areas is still lacking, we view this paper as stimulation for further discussion and research. Comprehensive comparative studies of the early Paleozoic ophiolites and metamorphic (particularly ultrahigh-pressure metamorphic) rocks in these Gondwana-derived terranes are urgently needed.

Acknowledgements

We thank Editor T. Mark Harrison for comments and editorial handling and two anonymous reviewers for constructive comments that have improved the quality of this paper. We also thank Zhengyu Chen, Li Su and Jian-hui Liu for their assistance in the laboratory operation of EPMA, LA–ICP–MS and SHRIMP dating. This study was jointly supported by the National Natural Science Foundation of China (Grant No. 41372066), Institute of Geology and Geological Survey Project of Chinese (Grant No. 1212011121243), the Strategic Priority Research Program (B) of the Chinese Academy of Sciences (Grant No. XDB03010600), the National Natural Science Foundation of China (No. 41025006) and the Guangzhou Institute of Geochemistry, Chinese Academy of Sciences (GIGCAS 135 project Y234021001). This is contribution No. IS-1946 from GIGCAS.

Appendix A. Supplementary material

Supplementary material related to this article can be found online at http://dx.doi.org/10.1016/j.epsl.2014.08.013.

References

Andersen, T., 2002. Correction of common lead in U–Pb analyses that do not report ^{204}Pb. Chem. Geol. 192 (1–2), 59–79.
Anovitz, L.M., 1991. Al zoning in pyroxene and plagioclase: window on late prograde to early retrograde P–T paths in granulite terranes. Am. Mineral. 76 (7–8), 1328–1343.
BGMR (Bureau of Geology and Mineral Resources of Xizang Autonomous Region), 1993. Regional Geology of Xizang (Tibet) Autonomous Region. Geological Publishing House, Beijing (in Chinese with English abstract).
Bhattacharya, A., Krishnakumar, K.R., Raith, M., Sen, S.K., 1991. An improved set of a-X parameters for Fe–Mg–Ca garnets and refinements of the orthopyroxene–garnet thermometer and the orthopyroxene–garnet–plagioclase–quartz barometer. J. Petrol. 32 (3), 629–656.
Black, L.P., Kamo, S.L., Allen, C.M., Aleinikoff, J.N., Davis, D.W., Korsch, R.J., Foudoulis, C., 2003. TEMORA 1: a new zircon standard for Phanerozoic U–Pb geochronology. Chem. Geol. 200 (1–2), 155–170.
Brown, M., 1993. P–T–t evolution of mountain belts and the causes of regional metamorphism. J. Geol. Soc. 150, 227–241.
Brown, M., 2001. From microscope to mountain belt: 150 years of petrology and its contribution to understanding geodynamics, particularly the tectonics of orogens. J. Geodyn. 32, 115–164.
Brown, M., 2006. Duality of thermal regimes is the distinctive characteristic of plate tectonics since the Neoarchean. Geology 34, 961–964.
Brown, M., 2007. Metamorphic conditions in orogenic belts: a record of secular change. Int. Geol. Rev. 49, 193–234.
Cao, Y.T., Liu, L., Wang, C., Kang, L., Yang, W.Q., Liang, S., Liao, X.Y., Wang, Y.W., 2013. Determination and implication of the HP pelitic granulite from the Munabulake area in the South Altyn Tagh. Acta Petrol. Sin. 29 (5), 1727–1739 (in Chinese with English abstract).
Carswell, D.A., O'Brien, P.J., 1993. Thermobarometry and geotectonic significance of high-pressure granulites: examples from the Moldanubian zone of the Bohemian massif in Lower Austria. J. Petrol. 34 (3), 427–459.
Catlos, E.J., Harrison, T.M., Manning, C.E., Grove, M., Rai, S.M., Hubbard, M.S., Upreti, B.N., 2002. Records of the evolution of the Himalayan orogen from in situ Th–Pb ion microprobe dating of monazite: Eastern Nepal and western Garhwal. J. Asian Earth Sci. 20 (5), 459–479.
Cawood, P.A., Buchan, C., 2007. Linking accretionary orogenesis with supercontinent assembly. Earth-Sci. Rev. 82, 217–256.
Cawood, P.A., Johnson, M.R.W., Nemchin, A.A., 2007. Early Palaeozoic orogenesis along the Indian margin of Gondwana: tectonic response to Gondwana assembly. Earth Planet. Sci. Lett. 255, 70–84.
Chen, D.L., Sun, Y., Liu, L., 2007. Metamorphic age and its geological implication for country rocks of eclogites in the Yuka of the north Qaidam Mountains. Earth Sci. Front. 14, 107–116 (in Chinese with English abstract).
Chen, D.L., Liu, L., Sun, Y., Liou, J.G., 2009. Geochemistry and zircon U–Pb dating and its implications of the Yukahe HP/UHP terrane, the North Qaidam, NW China. J. Asian Earth Sci. 35, 259–272.
Cheng, H., Zhang, C., Vervoort, J.D., Li, X., Li, Q., Zheng, S., Cao, D., 2011. Geochronology of the transition of eclogite to amphibolite facies metamorphism in the North Qinling orogen of central China. Lithos 125 (3), 969–983.
Cheng, H., Zhang, C., Vervoort, J.D., Li, X., Li, Q., Wu, Y., Zheng, S., 2012. Timing of eclogite facies metamorphism in the North Qinling by U–Pb and Lu–Hf geochronology. Lithos 136, 46–59.
Clarke, G.L., Klepeis, K.A., Daczko, N.R., 2000. Cretaceous high-P granulites at Milford Sound, New Zealand: metamorphic history and emplacement in a cobergent margin setting. J. Metamorph. Geol. 18, 359–374.
Compston, W., Williams, I.S., Kirschvink, J.L., Zichao, Z., Guogan, M.A., 1992. Zircon U–Pb ages for the early Cambrian time-scale. J. Geol. Soc. 149, 171–184.
Cong, B.L., Wu, G.Y., Zhang, Q., Zhang, R.Y., Zhai, M.G., Zhao, D.S., Zhang, W.H., 1993. Petrotectonic evolution of the Tethys zone in western Yunnan, China. Sci. China Ser. B 23 (11), 1201–1207 (in Chinese with English abstract).
Cooke, R.A., 2000. High-pressure temperature metamorphism in the St. Leonhard Granulite Massif, Austria: evidence from intermediate pyroxene-bearing granulites. Geol. Rundsch. 89, 631–651.
Debon, F., Le Fort, P., Sheppard, S.M.F., Sonet, J., 1986. The four plutonic belts of the Transhimalaya–Himalaya: a chemical, mineralogical, isotopic and chronological synthesis along a Tibet–Nepal section. J. Petrol. 27, 219–250.
Dewey, J.F., Shackelton, R.M., Chengfa, C., Yiyin, S., 1988. The tectonic evolution of the Tibetan Plateau. Philos. Trans. R. Soc. Lond. Ser. A 327, 379–413.
Eckert, J.O., Newton, R.C., Kleppa, O.J., 1991. The H of reaction and recalibration of garnet–pyroxene–plagioclase–quartz geobarometers in the CMAS system by solution calorimetry. Am. Mineral. 76 (1–2), 148–160.

Ellis, D.J., Green, D.H., 1979. An experimental study of the effect of Ca upon garnet–clinopyroxene Fe–Mg exchange equilibria. Contrib. Mineral. Petrol. 71 (1), 13–22.
England, P.C., Thompson, A.B., 1984. Pressure–temperature–time paths of regional metamorphism, I. Heat transfer during the evolution of regions of thickened continental crust. J. Petrol. 25, 894–928.
Ernst, W.G., Liou, J.G., 2008. High- and ultrahigh-pressure metamorphism: past results and future prospects. Am. Mineral. 93, 1771–1786.
Ferrari, O.M., Hochard, C., Stampfli, G.M., 2008. An alternative plate tectonic model for the Palaeozoic–Early Mesozoic Palaeotethyan evolution of Southeast Asia (Northern Thailand–Burma). Tectonophysics 451, 346–365.
Gehrels, G.E., Yin, A., Wang, X.F., 2003a. Detrital zircon geochronology of the northeastern Tibetan Plateau. Geol. Soc. Am. Bull. 115 (7), 881–896.
Gehrels, G.E., Yin, A., Wang, X.F., 2003b. Magmatic history of the northeastern Tibetan Plateau. J. Geophys. Res., Solid Earth 108 (B9) (1978–2012).
Gehrels, G., Kapp, P., DeCelles, P., Pullen, A., Blakey, R., Weislogel, A., Ding, L., Guynn, J., Martin, A., McQuarrie, N., Yin, A., 2011. Detrital zircon geochronology of pre-Tertiary strata in the Tibetan–Himalayan orogen. Tectonics 30 (5), TC5016. http://dx.doi.org/10.1029/2011TC002868.
Graham, C.M., Powell, R., 1984. A garnet–hornblende geothermometer: calibration, testing and application to the Pelona Schist, Southern California. J. Metamorph. Geol. 2, 13–31.
Green, D.H., Ringwood, A.E., 1967. An experimental investigation of the gabbro to eclogite transformation and its petrological applications. Geochim. Cosmochim. Acta 31, 767–833.
Guo, J.H., O'Brien, P.J., Zhai, M.G., 2002. High-pressure granulites in the Sanggan area, North China Craton: metamorphic evolution, P–T paths and geotectonic significance. J. Metamorph. Geol. 20, 741–756.
Harley, S.L., 1984. An experimental study of the partitioning of Fe and Mg between garnet and orthopyroxene. Contrib. Mineral. Petrol. 86, 359–373.
Harley, S.L., 1989. The origins of granulites: a metamorphic perspective. Geol. Mag. 126, 1059–1095.
Harley, S.L., 1992. Proterozoic granulite terranes. In: Condie, K. (Ed.), Proterozoic Crustal Evolution. In: Developments in Precambrian Geology, vol. 10. Elsevier, Amsterdam, pp. 301–359.
Harley, S.L., 2008. Refining the P–T records of UHT crustal metamorphism. J. Metamorph. Geol. 26, 125–156.
Holland, T.J.B., 1980. The reaction albite jadeite + quartz determined experimentally in the range 600–1200 degrees C. Am. Mineral. 65, 129–134.
Hoskin, P.W.O., Black, L.P., 2000. Metamorphic zircon formation by solid-state recrystallization of protolith igneous zircon. J. Metamorph. Geol. 18 (4), 423–439.
Hu, P.Y., Li, C., Su, L., Li, C.B., Yu, H., 2010. Zircon U–Pb dating of granitic gneiss in Wugong Mountain area, central Qiangtang, Qinghai–Tibet plateau: age record of Pan-African movement and Indo-China movement. Geol. China 4, 1050–1061 (in Chinese with English abstract).
Hu, P.Y., Li, C., Wang, M., Xie, C.M., Wu, Y.W., 2013. Cambrian volcanism in the Lhasa terrane, southern Tibet: record of an early Paleozoic Andean-type magmatic arc along the Gondwana proto-Tethyan margin. J. Asian Earth Sci. 77, 91–107.
Jackson, S.E., Pearson, N.J., Griffin, W.L., Belousova, E.A., 2004. The application of laser ablation-inductively coupled plasma-mass spectrometry to in situ U–Pb zircon geochronology. Chem. Geol. 211 (1–2), 47–69.
Jin, X.C., 2002. Permo-Carboniferous sequences of Gondwana affinity in southwest China and their paleogeographic implications. J. Asian Earth Sci. 20 (6), 633–646.
Kapp, P., Yin, A., Manning, C.E., Murphy, M., Harrison, T.M., Spurlin, M., Lin, D., Deng, X.G., Wu, C.M., 2000. Blueschist-bearing metamorphic core complexes in the Qiangtang block reveal deep crustal structure of northern Tibet. Geology 28 (1), 19–22.
Kapp, P., Yin, A., Manning, C.E., Harrison, T.M., Taylor, M.H., Ding, L., 2003. Tectonic evolution of the early Mesozoic blueschist-bearing Qiangtang metamorphic belt, central Tibet. Tectonics 22 (4), 1043. http://dx.doi.org/10.1029/2002TC001386.
Kohn, M.J., Spear, F.S., 1990. Two new geobarometers for garnet amphibolites, with applications to southeastern Vermont. Am. Mineral. 75, 89–96.
Krogh, E.J., 1988. The garnet–clinopyroxene Fe–Mg geothermometer—a reinterpretation of existing experimental data. Contrib. Mineral. Petrol. 99 (1), 44–48.
Kumar, C.R.R., Chacko, T., 1994. Geothermobarometry of mafic granulites and metapelite from the Palhat Gap, South India: petrological evidence for isothermal uplift and rapid cooling. J. Metamorph. Geol. 12 (4), 479–492.
Leake, B.E., Woolley, A.R., Arps, C.E.S., Birch, W.D., Gilbert, M.C., Grice, J.D., Hawthorne, F.C., Kato, A., Kisch, H.J., Krivovichev, V.G., Linthout, K., Laird, J., Mandarino, J.A., Maresch, W.V., Nickel, E.H., Rock, N.M.S., Schumacher, J.C., Smith, D.C., Stephenson, N.C.N., Ungaretti, L., Whittaker, E.J.W., Guo, Y.Z., 1997. Nomenclature of amphiboles: report of the subcommittee on amphiboles of the International Mineralogical Association, Commission on New Minerals and Mineral Names. Can. Mineral. 35, 219–246.
Lehmann, B., Zhao, X., Zhou, M., Du, A., Mao, J., Zeng, P., Kunst, F.H., Heppe, K., 2013. Mid-Silurian back-arc spreading at the northeastern margin of Gondwana: the Dapingzhang dacite-hosted massive sulfide deposit, Lancangjiang zone, southwestern Yunnan, China. Gondwana Res. 24 (2), 648–663.
Leier, A.L., Kapp, P., Gehrels, G.E., DeCelles, P.G., 2007. Detrital zircon geochronology of Carboniferous–Cretaceous strata in the Lhasa terrane, Southern Tibet. Basin Res. 19 (3), 361–378.
Li, C., 1987. The Longmu Co–Shuanghu–Lancangjiang plate suture and the north boundary of distribution of Gondwana affinity Permian–Carboniferous system in northern Tibet, China. J. Changchun Univ. Earth Sci. 17 (2), 155–166 (in Chinese with English abstract).
Li, C., Zheng, A., 1993. Paleozoic stratigraphy in the Qiangtang region of Tibet: relations of the Gondwana and Yangtze continents and ocean closure near the end of the Carboniferous. Int. Geol. Rev. 35 (9), 797–804.
Li, C., Cheng, L.R., Hu, K., Yang, Z.R., Hong, Y.R., 1995. Study on the Paleo-Tethys Suture Zone of Longmu Co–Shuanghu, Tibet. Geological Publishing House, Beijing (in Chinese with English abstract).
Li, C., Zhai, Q.G., Dong, Y.S., Huang, X.P., 2006. Discovery of eclogite and its geological significance in Qiangtang area, central Tibet. Chin. Sci. Bull. 51 (9), 1095–1100.
Li, C., Dong, Y.S., Zhai, Q.G., Wang, L.Q., Yan, Q.R., Wu, Y.W., He, T.T., 2008. Discovery of Eopaleozoic ophiolite in the Qiangtang of Tibet Plateau: evidence from SHRIMP U–Pb dating and its tectonic implications. Acta Petrol. Sin. 24 (1), 31–36 (in Chinese with English abstract).
Liang, X., Wang, G.H., Yuan, G.L., Liu, Y., 2012. Structural sequence and geochronology of the Qomo Ri accretionary complex, Central Qiangtang, Tibet: implications for the Late Triassic subduction of the Paleo-Tethys Ocean. Gondwana Res. 22 (2), 470–481.
Liu, F.L., Xu, Z.Q., Xue, H.M., 2004. Tracing the protolith, UHP metamorphism, and exhumation ages of orthogneiss from the SW Sulu terrane (eastern China): SHRIMP U–Pb dating of mineral inclusion-bearing zircons. Lithos 78 (4), 411–429.
Liu, L., Yang, J.X., Chen, D.L., Wang, C., Zhang, C.L., Yang, W.Q., Cao, Y.T., 2010. Progress and controversy in the study of HP–UHP metamorphic terranes in the West and Middle Central China orogen. J. Earth Sci. 21, 581–597.
Liu, L., Wang, C., Cao, Y.T., Chen, D.L., Kang, L., Yang, W.Q., Zhu, X.H., 2012. Geochronology of multi-stage metamorphic events: constraints on episodic zircon growth from the UHP eclogite in the South Altyn, NW China. Lithos 136, 10–26.
Liu, P.H., Liu, F.L., Liu, C.H., Wang, F., Liu, J.H., Yang, H., Cai, J., Shi, J.R., 2013. Petrogenesis, P–T–t path, and tectonic significance of high-pressure mafic granulites from the Jiaobei terrane, North China Craton. Precambrian Res. 233, 237–258.
Liu, X.C., Hu, J.M., Zhao, Y., Lou, Y.X., Wei, C.J., Liu, X.H., 2009. Late Neoproterozoic/Cambrian high-pressure mafic granulites from the Grove Mountains, East Antarctica: P–T–t path, collisional orogeny and implications for assembly of East Gondwana. Precambrian Res. 174, 181–199.
Liu, Y., Zhong, D.L., 1997. Petrology of high-pressure granulites from the eastern Himalayan syntaxis. J. Metamorph. Geol. 15 (4), 451–466.
Liu, Y., Santosh, M., Zhao, Z.B., Niu, W.C., Wang, G.H., 2011. Evidence for palaeo-Tethyan oceanic subduction within central Qiangtang, northern Tibet. Lithos 127 (1–2), 39–53.
Ludwig, K.R., 1999. Using Isoplot/EX, Version 2.01. A Geochronological Toolkit for Microsoft Excel. Special Publication, vol. 1a. Berkeley Geochronological Center, p. 47.
Ludwig, K.R., 2001. Squid1.02: A User's Manual. Special Publication, vol. 2. Berkeley Geochronological Center, p. 19.
Ludwig, K.R., 2003. User's Manual for Isoplot 3.00. A Geochronological Toolkit for Microsoft Excel. Special Publication, vol. 4a. Berkeley Geochronology, Center, Berkeley, CA.
Metcalfe, I., 2006. Palaeozoic and Mesozoic tectonic evolution and palaeogeography of East Asian crustal fragments: the Korean Peninsula in context. Gondwana Res. 9, 24–46.
Metcalfe, I., 2011a. Palaeozoic–Mesozoic history of SE Asia. In: Hall, R., Cottam, M., Wilson, M. (Eds.), The SE Asian Gateway: History and Tectonics of Australia–Asia Collision. Geol. Soc. (Lond.) Spec. Publ. 355, 7–35. http://dx.doi.org/10.1144/SP355.2.
Metcalfe, I., 2011b. Tectonic framework and Phanerozoic evolution of Sundaland. Gondwana Res. 19, 3–21.
Metcalfe, I., 2013. Gondwana dispersion and Asian accretion: tectonic and palaeogeographic evolution of eastern Tethys. J. Asian Earth Sci. 66, 1–33.
Miller, C., Thöni, M., Frank, W., Grasemann, B., Klötzli, U., Guntli, P., Draganits, E., 2001. The early Palaeozoic magmatic event in the Northwest Himalaya, India: source, tectonic setting and age of emplacement. Geol. Mag. 138 (03), 237–251.
Mints, M.V., Belousova, E.A., Konilov, A.N., Natapov, L.M., Shchipansky, A.A., Griffin, W.L., O'Reilly, S.Y., Dokukina, K.A., Kaulina, T.V., 2010. Mesoarchean subduction processes: 2.87 Ga eclogites from the Kola Peninsula, Russia. Geology 38 (8), 739–742.
Möller, A., Mezeger, K., Schenk, V., 2000. U–Pb dating of metamorphic minerals: PanAfrican metamorphism and prolonged slow cooling of high-pressure granulites in Tanzania, East Africa. Precambrian Res. 104, 123–146.
Newton, R.C., Perkins, D., 1982. Thermodynamic calibration of geobarometers based on the assemblages garnet–plagioclase–orthopyroxene (clinopyroxene)–quartz. Am. Mineral. 67 (2), 203–222.
O'Brien, P.J., Rötzler, J., 2003. High-pressure granulites: formation, recovery of peak conditions and implications for tectonics. J. Metamorph. Geol. 21 (1), 3–20.
Powell, R., 1985. Regression diagnostics and robust regression in geothermometer/geobarometer calibration: the garnet–clinopyroxene geothermometer revisited. J. Metamorph. Geol. 3 (3), 231–243.

Pullen, A., Kapp, P., Gehrels, G.E., Vervoort, J.D., Ding, L., 2008. Triassic continental subduction in central Tibet and Mediterranean-style closure of the Paleo-Tethys Ocean. Geology 36 (5), 351–354.
Pullen, A., Kapp, P., Gehrels, G.E., Ding, L., Zhang, Q.H., 2011. Metamorphic rocks in central Tibet: lateral variations and implications for crustal structure. Geol. Soc. Am. Bull. 123, 585–600.
Ravna, E.K., 2000. Distribution of Fe^{2+} and Mg between coexisting garnet and hornblende in synthetic and natural systems: an empirical calibration of the garnet–hornblende Fe–Mg geothermometer. Lithos 53 (3–4), 265–277.
Rong, J.Y., Boucot, A.J., Su, Y.Z., Strusz, D.L., 1995. Biogeographical analysis of Late Silurian brachiopod faunas, chiefly from Asia and Australia. Lethaia 28, 39–60.
Rubatto, D., Hermann, J., 2003. Zircon formation during fluid circulation in eclogites (Monviso, Western Alps): implications for Zr and Hf budget in subduction zones. Geochim. Cosmochim. Acta 67 (12), 2173–2187.
Rubatto, D., Gebauer, D., Compagnoni, R., 1999. Dating of eclogite-facies zircons: the age of Alpine metamorphism in the Sesia–Lanzo Zone (Western Alps). Earth Planet. Sci. Lett. 167 (3), 141–158.
Salje, E., 1986. Heat capacities and entropies of andalusite and sillimanite. The influence of fibrolitisation on the phase diagram of the Al_2SiO_5 polymorphs. Am. Mineral. 71, 1366–1371.
Sobel, E.R., Arnaud, N., 1999. A possible middle Paleozoic suture in the Altyn Tagh, NW China. Tectonics 18 (1), 64–74.
Song, S., Zhang, L., Niu, Y., Su, L., Song, B., Liu, D., 2006. Evolution from oceanic subduction to continental collision: a case study from the Northern Tibetan Plateau based on geochemical and geochronological data. J. Petrol. 47 (3), 435–455.
Spear, F.S., 1993. Metamorphic Phase Equilibria and Pressure–Temperature–Time Paths. Monograph Series. Mineralogical Society of America, Washington, DC.
Stampfli, G.M., Borel, G.D., 2002. A plate tectonic model for the Paleozoic and Mesozoic constrained by dynamic plate boundaries and restored synthetic oceanic isochrones. Earth Planet. Sci. Lett. 196, 17–33.
Sun, S.S., McDonough, W.F., 1989. Chemical and isotopic systematics of oceanic basalt: implications for mantle composition and processes. In: Saunders, A.D., Norry, M.J. (Eds.), Magmatism in the Ocean Basins. Geol. Soc. (Lond.) Spec. Publ. 42, 528–548.
Tapponnier, P., Mercier, J.L., Proust, F., Andrieux, J., Armijo, R., Bassoullet, J.P., Brunel, M., Burg, J.P., Colchen, M., Dupre, B., Girardeau, J., Marcoux, J., Mascle, G., Matte, P., Nicolas, A., Tingdong, L., Xuchang, X., Chenfa, C., Paoyu, L., Guangcen, L., Naiwen, W., Guoming, C., Tonglin, H., Xibin, W., Wanming, D., Haixiang, Z., Huaibin, S., Yongong, C., Ji, Z., Hongrong, Q., 1981. The Tibetan side of the India–Eurasia collision. Nature 294 (5840), 405–410.
Thost, D.E., Hensen, B.J., Motoyoshi, Y., 1991. Two-stage decompression in garnet-bearing mafic granulites from Sostrene Island, Prydz Bay, East Antarctica. J. Metamorph. Geol. 9, 245–256.
Vavra, G., Schmid, R., Gebauer, D., 1999. Internal morphology, habit and U–Th–Pb microanalysis of amphibolite-to-granulite facies zircons: geochronology of the Ivrea Zone (Southern Alps). Contrib. Mineral. Petrol. 134 (4), 380–404.
Von Raumer, J., Stampfli, G., Borel, G., Bussy, F., 2002. Organization of pre-Variscan basement areas at the north-Gondwanan margin. Int. J. Earth Sci. 91, 35–52.
Wang, B.D., Wang, L.Q., Pan, G.T., Yin, F.G., Wang, D.B., Tang, Y., 2013. U–Pb zircon dating of Early Paleozoic gabbro from the Nantinghe ophiolite in the Changning–Menglian suture zone and its geological implication. Chin. Sci. Bull. 58 (8), 920–930.
Wang, H., Wu, Y.B., Gao, S., Liu, X.C., Gong, H.J., Li, Q.L., Li, X.H., Yuan, H.L., 2011. Eclogite origin and timings in the North Qinling terrane, and their bearing on the amalgamation of the South and North China Blocks. J. Metamorph. Geol. 29 (9), 1019–1031.
Wang, X.X., Zhang, J.J., Santosh, M., Liu, J., Yan, S.Y., Guo, L., 2012. Andean-type orogeny in the Himalayas of south Tibet: implications for early Paleozoic tectonics along the Indian margin of Gondwana. Lithos 154, 248–262.
Wu, Y.W., 2013. The evolution record of Longmuco–Shuanghu–Lancang ocean. Doctor Degree. College of Earth Sciences, Jilin University, Changchun.
Xie, L.W., Zhang, Y.B., Zhang, H.H., Sun, J.F., Wu, F.Y., 2008. In situ simultaneous determination of trace elements, U–Pb and Lu–Hf isotopes in zircon and baddeleyite. Chin. Sci. Bull. 53 (10), 1565–1573.
Yin, A., Harrison, T.M., 2000. Geologic evolution of the Himalayan–Tibetan orogen. Annu. Rev. Earth Planet. Sci. 28, 211–280.
Yin, A., Nie, S., 1996. A Phanerozoic palinspastic reconstruction of China and its neighboring regions. In: Yin, A., Harrison, T.M. (Eds.), The Tectonics of Asia. Cambridge Univ. Press, New York, pp. 442–485.
Yu, S.Y., Zhang, J.X., Gong, J.H., Li, Y.S., 2013. Research on HP granulite facies metamorphism and anatexis: a case study of Dulan area in the north Qaidam Mountains. Acta Petrol. Sin. 29 (6), 2061–2072 (in Chinese with English abstract).
Zhai, Q.G., Li, C., Huang, X.P., 2007. The fragment of Paleo-Tethys ophiolite from central Qiangtang, Tibet: geochemical evidence of metabasites in Guoganjianian. Sci. China, Ser. D, Earth Sci. 50 (9), 1302–1309.
Zhai, Q.G., Wang, J., Li, C., Su, L., 2010. SHRIMP U–Pb dating and Hf isotopic analyses of Middle Ordovician meta-cumulate gabbro in central Qiangtang, northern Tibetan plateau. Sci. China, Ser. D, Earth Sci. 53 (5), 657–664.
Zhai, Q.G., Jahn, B.M., Zhang, R.Y., Wang, J., Su, L., 2011a. Triassic subduction of the Paleo-Tethys in northern Tibet, China: evidence from the geochemical and isotopic characteristics of eclogites and blueschists of the Qiangtang Block. J. Asian Earth Sci. 42 (6), 1356–1370.
Zhai, Q.G., Zhang, R.Y., Jahn, B.M., Li, C., Song, S.G., Wang, J., 2011b. Triassic eclogites from central Qiangtang, northern Tibet, China: petrology, geochronology and metamorphic P–T path. Lithos 125 (1–2), 173–189.
Zhai, Q.G., Jahn, B.M., Wang, J., Su, L., Mo, X.X., Wang, K.L., Tang, S.H., Lee, H.Y., 2013. The Carboniferous ophiolite in the middle of the Qiangtang terrane, Northern Tibet: SHRIMP U–Pb dating, geochemical and Sr–Nd–Hf isotopic characteristics. Lithos 168, 186–199.
Zhang, J.X., Mattinson, C.G., Meng, F.C., Wan, Y.S., 2005. An Early Palaeozoic HP/HT granulite–garnet peridotite association in the south Altyn Tagh, NW China: P–T history and U–Pb geochronology. J. Metamorph. Geol. 23 (7), 491–510.
Zhang, J.X., Mattinson, C.C., Meng, F.C., Wan, Y.S., Dung, K.A., 2008. Polyphase tectonothermal history recorded in granulitized gneisses from the north Qaidam HP/UHP metamorphic terrane, western China: evidence from zircon U–Pb geochronology. Geol. Soc. Am. Bull. 12, 732–749.
Zhang, J.X., Yu, S.Y., Meng, F.C., Li, J.P., 2011. Polyphase early Paleozoic metamorphism in the northern Qinling orogenic belt. Acta Petrol. Sin. 27 (4), 1179–1190 (in Chinese with English abstract).
Zhang, X.Z., Dong, Y.S., Shi, J.R., Wang, S.Y., 2010a. The formation and significance of jadeite garnet mica schist newly discovered in Longmu Co–Shuanghu suture zone, Central Qiangtang. Earth Sci. Front. 17 (1), 93–103 (in Chinese with English abstract).
Zhang, X.Z., Dong, Y.S., Li, C., Chen, W., Shi, J.R., Zhang, Y., Wang, S.Y., 2010b. Identification of the elcogites in different ages and their tectonic significance in Central Qiangtang, Tibetan Plateau: constraints from $^{40}Ar/^{39}Ar$ isotope chronology. Geol. Bull. China 29 (12), 1815–1824 (in Chinese with English abstract).
Zhang, X.Z., Dong, Y.S., Li, C., Shi, J.R., Wang, S.Y., 2010c. Geochemistry and Tectonic significance of eclogites in Central Qiangtang, Tibetan Plateau. Geol. Bull. China 29 (12), 1804–1814 (in Chinese with English abstract).
Zhang, X.Z., Dong, Y.S., Li, C., Deng, M.R., Zhang, L., Xu, W., 2014. Tectonic setting and petrogenesis mechanism of late Triassic magmatism in Central Qiangtang, Tibetan Plateau: take the Xiangtaohu pluton in the Hongjishan region as an example. Acta Petrol. Sin. 30 (2), 547–564 (in Chinese with English abstract).
Zhang, Y.C., Yuan, T.X., Zhai, Q.G., 2009. A preliminary report of the fieldtrip on the Carboniferous–Permian sequences in the North and South of the Longmu Co–Shuanghu suture zone, Northern Tibet in May and June. Permophiles 53, 5–7.
Zhao, G.C., Cawood, P.A., Wilde, S.A., Lu, L., 2001. High-pressure granulites (retrograded eclogites) from the Hengshan Complax, North China Craton: petrology and tectonic implications. J. Petrol. 42, 1141–1170.
Zhu, D.C., Zhao, Z.D., Niu, Y.L., Dilek, Y., Wang, Q., Ji, W.H., Dong, G.C., Sui, Q.L., Liu, Y.S., Yuan, H.L., Mo, X.X., 2012. Cambrian bimodal volcanism in the Lhasa Terrane, southern Tibet: record of an early Paleozoic Andean-type magmatic arc in the Australian proto-Tethyan margin. Chem. Geol. 328, 290–308.
Zhu, D.C., Zhao, Z.D., Niu, Y., Dilek, Y., Hou, Z.Q., Mo, X.X., 2013. The origin and pre-Cenozoic evolution of the Tibetan Plateau. Gondwana Res. 23 (4), 1429–1454.
Zhu, T.X., Zhang, Q.Y., Dong, H., Wang, Y.J., Yu, Y.S., Feng, X.T., 2006. Discovery of the Late Devonian and Late Permian radiorian cherts in tectonic melanges in the Cedo Caka area, Shuanghu, northern Tibet, China. Geol. Bull. China 25 (12), 1413–1418 (in Chinese with English abstract).
Zong, K.Q., Zhang, Z.M., He, Z.Y., Hu, Z.C., Santosh, M., Liu, Y.S., Wang, W., 2012. Early Palaeozoic high-pressure granulites from the Dunhuang block, northeastern Tarim Craton: constraints on continental collision in the southern Central Asian Orogenic Belt. J. Metamorph. Geol. 30 (8), 753–768.